

Synthesis, elaboration and characterization of the new material CuIn_3S_5 thin films

N. Khémiri · M. Kanzari

Received: 3 March 2009 / Accepted: 9 July 2009 / Published online: 22 July 2009
© Springer Science+Business Media, LLC 2009

Abstract CuIn_3S_5 compound was prepared by direct reaction of high-purity elemental copper, indium and sulphur. CuIn_3S_5 thin films were prepared from powder by thermal evaporation under vacuum (10^{-6} mbar) onto glass substrates. The glass substrates were heated from 30 to 200 °C. The powder was characterized for their structural and compositional properties by using X-ray diffraction (XRD) and energy dispersive X-ray (EDAX). The XRD studies revealed that the powder exhibiting P-chalcopyrite structure. From the XRD data, we calculated the lattice parameters a and c . Then, the cation–anion bond lengths l_{AC} and l_{BC} are deduced. The films were characterized for their structural, compositional, morphological and optical properties by using XRD, EDAX, atomic force microscopy and optical measurement techniques (transmittance and reflectance). XRD analysis revealed that the films deposited at a room temperature (30 °C) are amorphous in nature, whereas those deposited on heated substrates (≥ 75 °C) were polycrystalline with a preferred orientation along (112) of the chalcopyrite phase. The surface morphological analysis revealed that the films grown at different substrate temperature had an average roughness between 1.1 and 4.8 nm. From the analysis of the transmission and reflection data, the values of direct and indirect band gap of the films were determined. We found that the optical band gap decreases when the substrate temperature increases.

Introduction

Development of thin film solar cells based on CuInSe_2 and the related compounds of $\text{CuSe-In}_2\text{Se}_3$ system viz., $\text{Cu}_2\text{In}_4\text{Se}_7$, CuIn_3Se_5 , CuIn_5Se_8 , etc., have made considerable progress in recent years [1]. Among them, CuIn_3S_5 has recently attracted much attention because it is expected to play an important role in the optimization of solar cells based on CuInSe_2 [2–4].

CuInS_2 is one of the Cu-In-VI_2 type semiconductors, which crystallize in the chalcopyrite structure. Its direct band gap of 1.5 eV, high absorption coefficient and environmental viewpoint that CuInS_2 does not contain any toxic constituents, in comparison with the frequently studied CuInSe_2 , makes it suitable for terrestrial photovoltaic applications [5]. However, in spite of these interesting properties, very little is known about the related compounds of $\text{CuS-In}_2\text{S}_3$ system. One of them is the ternary compound CuIn_3S_5 that has chalcopyrite structure and belongs to the In-rich side of the pseudo-binary $\text{CuS-In}_2\text{S}_3$ system [6]. Since this compound has the deficiency of one cation over the anions, it is called ‘ordered defect compounds’. The ordered defect compounds are the off-stoichiometric phases, located on the $\text{IVI-III}_2\text{VI}_3$ pseudo-binary tie line [7]. At the extreme limits of structural tolerance to off-stoichiometry of chalcopyrite phases, these compounds stabilize due to the ordering of the neutral defect pairs $2\text{V}_{\text{Cu}}^{-1} + \text{In}_{\text{Cu}}^{2+}$ and $2\text{Cu}_{\text{In}}^{-2} + \text{In}_{\text{Cu}}^{2+}$ in Cu-In-VI_2 phase [8].

Some papers [9–13] indicated the presence of the CuIn_3S_5 phase in the near-surface region of CuInS_2 thin films but in our knowledge, no papers dealing with the physical properties of this compound have been reported.

In this study, we present results concerning the fabrication of the CuIn_3S_5 thin films made by the thermal

N. Khémiri (✉) · M. Kanzari
Laboratoire de Photovoltaïque et Matériaux Semi-conducteurs,
ENIT, BP 37, Le belvédère, 1002 Tunis, Tunisia
e-mail: naoufel_khemiri@yahoo.fr

evaporation method and the characterization of the structural, compositional, morphological and optical properties of these films.

Experimental procedure

Synthesis of CuIn_3S_5

The CuIn_3S_5 crystal has been synthesized by direct reaction of high-purity (99.999%) elemental copper, indium and sulphur. Stoichiometric amounts of the elements Cu, In and S, corresponding to the composition of the ternary compound, were placed in a quartz ampoule about 170 mm in length with diameter 20 mm, which were chemically cleaned with a mixture of acids $\text{HNO}_3/\text{HCl} = 1:3$, rinsing in distilled water and annealing for 2 h at 300 °C. After pumping down to 10^{-5} mbar, the ampoules were sealed off and transferred to a programmable furnace (Nabertherm-Allemagne). For the synthesis, the temperature of the furnace was raised to 600 °C with a rate of 10 °C/h and the temperature was kept constant at 600 °C for 24 h. Then, the temperature was increased with the rate 20 °C/h up to 1000 °C. A complete homogenization could be obtained by keeping the melt at this temperature (1000 °C) for about 48 h. Finally, the temperature was lowered to 800 °C at a rate of 10 °C/h and the furnace was switched off until the tube reached room temperature. The crystals obtained by this method had a diameter of 12 mm and a length of around 30 mm.

Film preparation

Thin films of CuIn_3S_5 were prepared by thermal evaporation from a Tungsten boat on heated and non-heated glass substrates (Corning 7059) of rectangular shape ($2.5 \times 1.5 \text{ cm}^2$) under vacuum (10^{-6} mbar) using a high vacuum coating unit Alcatel. The substrates were placed directly above the source at a distance of 15 cm and were heated by an insulator heater system, and the substrate temperature (T_s) was measured using a thermocouple embedded in the substrate holder underneath the substrates. The glass substrates were previously cleaned with washing agents (commercial detergent, acetone, ethanol and deionized water) before being introduced into the vacuum system. The base pressure of the vacuum system was kept between 10^{-5} and 10^{-6} mbar.

Characterization of powder and the thin films

The crystalline phase and crystal orientation of the powder and the prepared films were examined using Philips X'Pert X-ray diffractometer. $\text{CuK}\alpha$ ($\lambda = 1.54056 \text{ \AA}$) radiation was used. The high tension and current were 40 kV and

30 mA, respectively. Normal incidence transmittance (T) and reflectance (R) spectra were recorded at room temperature in the range from 300 to 1800 nm using a double-beam spectrophotometer, model SHIMADZU UV 3100S. The films' thickness was calculated from the positions of the interference maxima and minima of reflectance spectra using a standard method [14]. The composition of the films and the powder were determined by means of energy dispersive X-ray analysis (EDAX) using a JEOL 6700F. The surface morphology of the films was probed with the atomic force microscopy (AFM). The hot probe method's measurements were carried out in order to determine the conductivity types of the samples.

Results and discussion

Characterization of powder

X-ray diffraction (XRD) pattern obtained for the powder of CuIn_3S_5 is presented in Fig. 1. The sharp peaks present in the pattern indicate the polycrystalline nature of the sample [7]. The analysis of this pattern showed that the peak at $2\theta = 27.88^\circ$ due to the (112) plane has the highest intensity. Comparing the XRD pattern (Fig. 1) of the CuIn_3S_5 single crystal powder with this of CuInS_2 [15], we notice that the XRD pattern of the CuIn_3S_5 is very similar to this of CuInS_2 with a chalcopyrite structure, except the presence of four additional peaks at $2\theta = 23.74^\circ$, 30.53° , 32.56° and 36.88° . These additional reflections due to (110), (200), (202) and (114) planes are characteristic of ordered defect chalcopyrites (ODC) [16], with spatial group $P-42c$ called P-chalcopyrite. The main difference between the chalcopyrite (CuInS_2) and the P-chalcopyrite (CuIn_3S_5) structures is an ordered exchange of two Cu atoms by two In atoms in the 2d positions of the unit cell

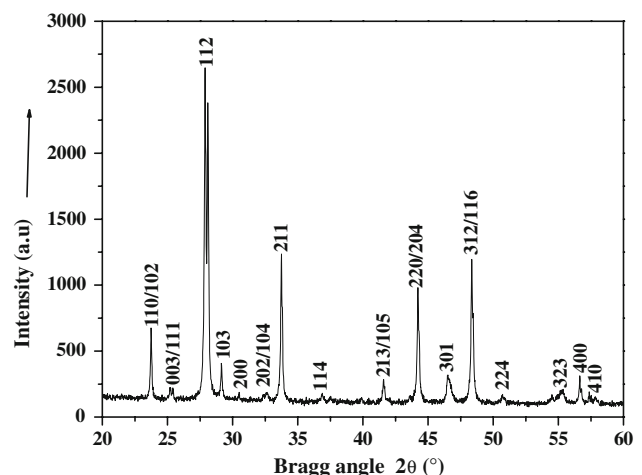


Fig. 1 XRD spectra of CuIn_3S_5 powder

Table 1 Structural parameters of the prepared powder of CuIn₃S₅

Peak no.	<i>III</i> _{max} (%)	2θ (°)	<i>d</i> _{hkl} (Å)	<i>hkl</i>
1	22	23.74	3.74	110
2	4.3	25.41	3.50	003/111
3	100	27.88	3.20	112
4	10.5	29.14	3.06	103
5	2.8	30.53	2.93	200
6	3.1	32.56	2.75	202
7	45	33.75	2.65	211
8	3.2	36.88	2.44	114
9	7.3	41.58	2.17	213/105
10	32	44.22	2.05	204/220
11	8.8	46.55	1.95	301
12	43.4	48.35	1.88	312/116
13	3.4	50.72	1.80	224
14	4.1	55.27	1.66	323
15	7.6	56.65	1.62	400
16	3.9	57.37	1.61	410

[17, 18]. These structural properties are very important. Indeed, the chalcopyrite phase and (112) orientation are reported to be beneficial to efficient solar energy conversion [19]. The Miller indices (*hkl*), the diffraction angles (2θ), the interplanar spacings (*d*) and relative intensity (*III*_{max}) for the diffractogram of the powder of CuIn₃S₅ were presented in Table 1. The lattice parameters *a* and *c* of CuIn₃S₅ powder were calculated by using the following relation:

$$\frac{1}{d^2} = \frac{h^2 + k^2}{a^2} + \frac{l^2}{c^2} \tag{1}$$

where *d* is interplanar spacing determined using Bragg’s equation and *h*, *k*, *l* are the miller indices of the lattice planes. We found 5.82 and 11.58 Å, respectively. From these values and by using the following relationships [20],

$$\sigma = 0.5 - 0.25(c^2/2a^2 - 1)^{1/2}$$

$$l_{AC} = 0.125a [64\sigma^2 + 4 + (c/a)^2]^{1/2} \tag{2}$$

$$l_{BC} = 0.125a [64(0.5 - \sigma)^2 + 4 + (c/a)^2]^{1/2}$$

We calculated the positional parameter σ , which characterizes the position of C atoms with respect to A and B atoms in the chalcopyrite structure the A^IB^{III}C₂^{VI} and the nearest neighbour anion–cation bond lengths (*l*_{AC}) and (*l*_{BC}) [21]. We found 0.252, 2.52 and 2.50 Å, respectively. The atomic ratios of elements quantitative analysis using EDAX were employed in this study to analyze the atomic ratios of Cu, In and S in the prepared powder. The atomic ratios of elements and the composition of CuIn₃S₅ powder are shown in Table 2. The composition of CuIn₃S₅ powder

Table 2 Chemical composition of CuIn₃S₅ powder

Cu (at.%)		In (at.%)		S (at.%)		Composition
Cal	Obs	Cal	Obs	Cal	Obs	
11.11	12.65	33.33	30.75	55.55	56.59	Cu _{1.13} In _{2.78} S _{5.09}

is fairly close to the ideal theoretical value of the starting composition. On the other hand, EDAX analysis made at several zones of the powder did not show any observable variation of the stoichiometric constituents of the elements, thereby suggesting the homogeneous nature of the powder.

CuIn₃S₅ thin films characterization

Structural properties

The X-ray diffractograms corresponding to the CuIn₃S₅ thin films deposited at different heated substrates are showed in Fig. 2. It is clear that the film deposited on no heated substrate (*T*_s = 30 °C) is amorphous in nature, whereas those deposited on heated substrates (≥75 °C) are polycrystalline in nature with a preferred orientation along the CuIn₃S₅ (112) plane, which indicates that the crystallites are oriented preferentially parallel to the plane of the glass substrate. The amorphous nature of the film formed at low substrate temperature is due to the non-availability of sufficient thermal energy for the diffusion of adatoms on the substrate surface for the nucleation [22]. It is observed that crystallinity of the films increases by increasing the temperature growth.

The average grain size (*L*) of the films was evaluated from the XRD peak of (112) by using Scherrer’s relation [23]:

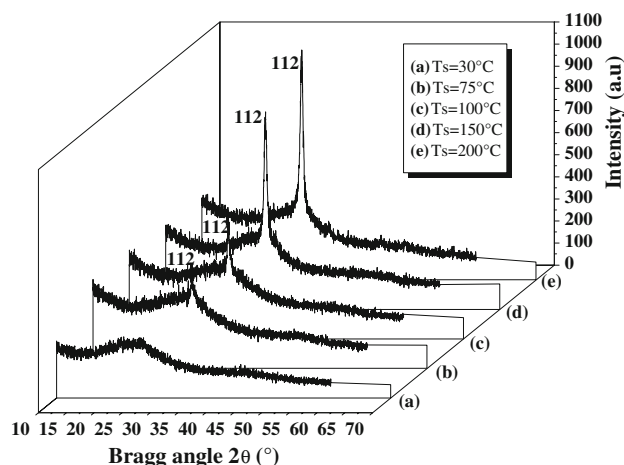


Fig. 2 XRD patterns of CuIn₃S₅ films deposited at different substrate temperatures

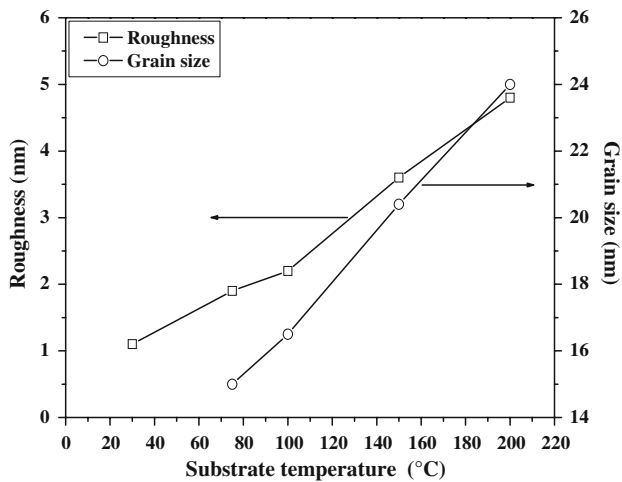


Fig. 3 Roughness and grain size of CuIn_3S_5 films deposited at different substrate temperatures

$$L = \frac{0.9\lambda}{\beta \cos \theta} \quad (3)$$

where λ is the X-ray wavelength, β is the full-width at half-maximum of the (112) diffraction line and θ is the diffraction angle of the XRD spectra. The average grain size increases from 15 to 24 nm by increasing the temperature growth from 30 to 200 °C, respectively (Fig. 3), which is due to improvement in the crystallinity of the films. It is clear that the substrate temperature has a great effect on the crystallinity of the films.

Compositional and morphological studies

EDAX measurements were carried out on different zones of the film surfaces to confirm the presence of Cu, In and S atoms and to determine their average content. Figure 4 shows the typical composition profile of Cu, In and S versus variation of substrate temperature growth. It is clear that the average atomic composition is near the stoichiometric formula CuIn_3S_5 . This analysis revealed that the substrate temperature has not significant effect on the film compositions. The small deviation of CuIn_3S_5 films' compositions compared with that of powder composition might be due to the slight decomposition of the starting material during the evaporation or due to the difference in the vapour pressures of the constituent elements of the compound [24]. Figure 5 shows AFM images of the CuIn_3S_5 films deposited at room temperature and at 75, 100, 150, 200 °C. The films exhibited a different morphology of surface grains, which are dependent on the substrate temperature. The surfaces of the films deposited at room temperature and at 75 °C are smooth due to poor crystallinity. Indeed, from XRD analysis it has been shown that the films in this case are globally amorphous.

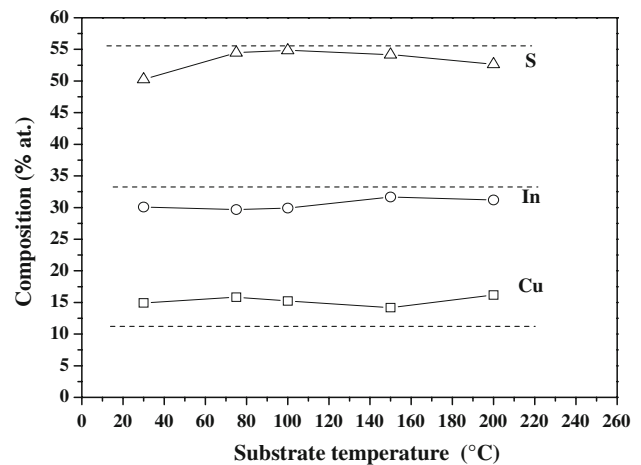


Fig. 4 Chemical compositions of CuIn_3S_5 films deposited at different substrate temperatures

However, the films with T_s equal to 100, 150 and 200 °C are homogeneous and are constituted of densely packed grains. The root mean square (RMS) values of surface roughness were found between 1.1 and 4.8 nm (Fig. 3). The roughness of the films shows distinct increase by increasing the substrate temperature. It has been shown that rougher surfaces constituted by larger grains can advance optical scattering making to increase the absorption coefficient [25].

Optical properties

Figures 6 and 7 show the typical transmission (T) and reflection (R) spectra of CuIn_3S_5 films, in the wavelength range of 300–1800 nm, grown on different temperatures substrates. It is clear from Fig. 6 that the transmittance spectrum shows interference fringes with a sharp fall at the band edge in the region of 900–1800 nm, whereas the interference effects disappear in the region of very strong absorption, maximum amplitude is obtained in the transparent region. The appearance of interference maxima and minima at the same wavelength position indicates the optical homogeneity of the deposited films. The optical transmittance of the films (at wavelength >900 nm) increased from 77 to 88% with the increase in substrate temperature from 30 to 150 °C and then decreased to 62% when T_s is equal to 200 °C. This decrease is probably due to the increase in surface roughness of films with substrate temperature shown in the AFM images [26]. The optical absorption coefficient was evaluated from the transmittance (T) and reflectance (R) data by using the following formula [27]:

$$\alpha = \frac{1}{d} \ln \left(\frac{(1-R)^2}{T} \right) \quad (4)$$

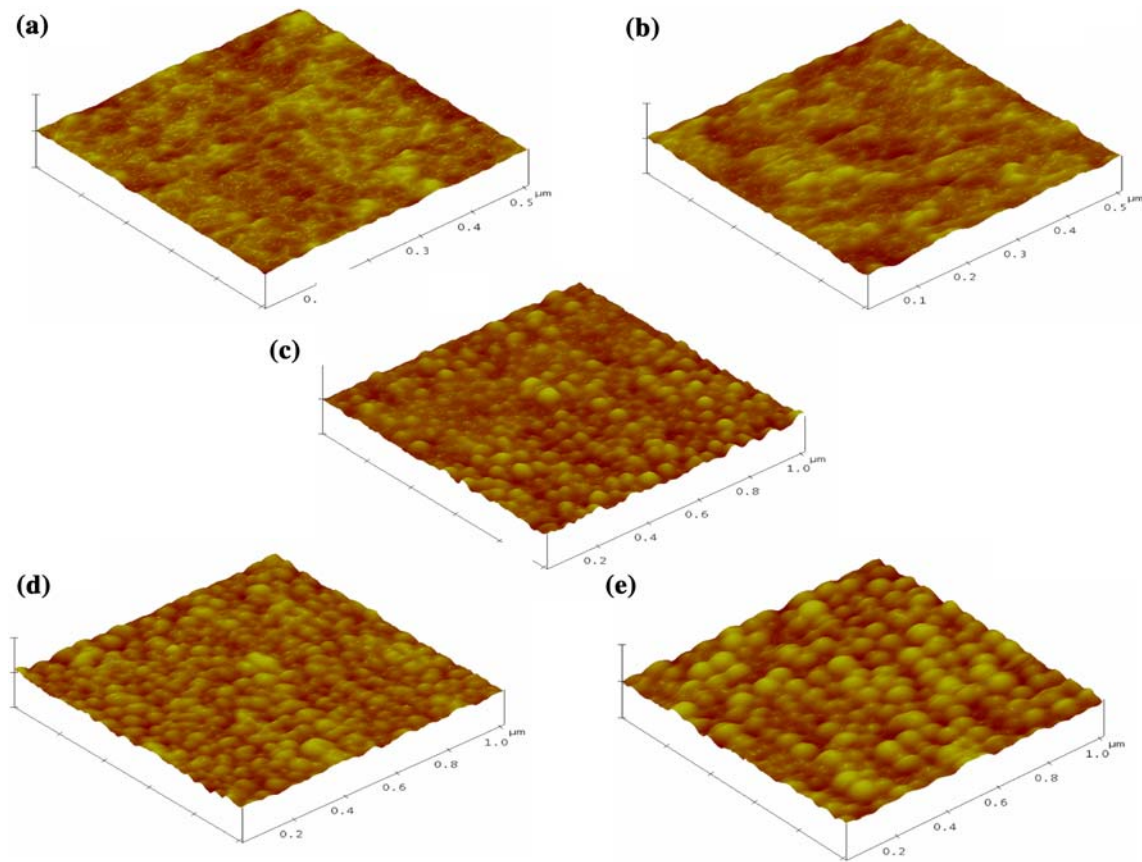


Fig. 5 AFM images of CuIn_3S_5 films deposited at different substrate temperatures: **a** 30 °C, **b** 75 °C, **c** 100 °C, **d** 150 °C and **e** 200 °C

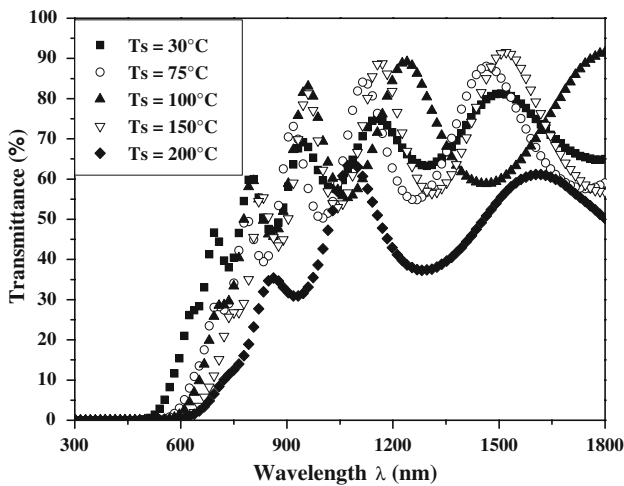


Fig. 6 Optical transmittance spectra of CuIn_3S_5 films deposited at different substrate temperatures

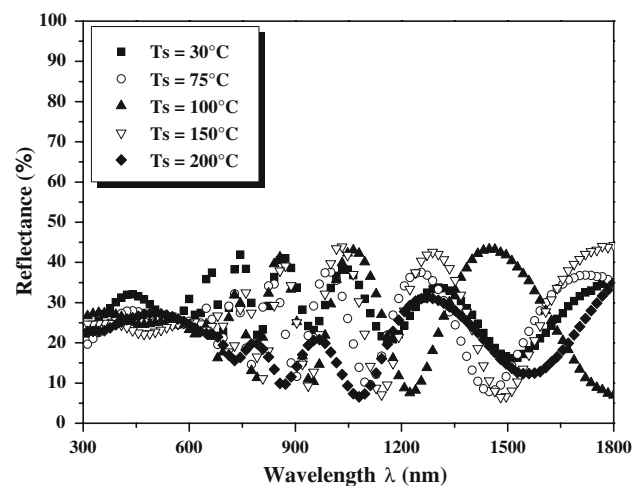


Fig. 7 Optical reflectance spectra of CuIn_3S_5 films deposited at different substrate temperatures

where α is the absorption coefficient and d is the film thickness. It is clear from Fig. 8 that the absorption coefficient increases by increasing the substrate temperature in the visible spectral range. The increase in the absorption coefficient can be explained by the increase in roughness of

the films by increasing the substrate temperature. This result is very important because we know that the spectral dependence of the absorption coefficient affects the solar cell conversion efficiency for photovoltaic applications [28].

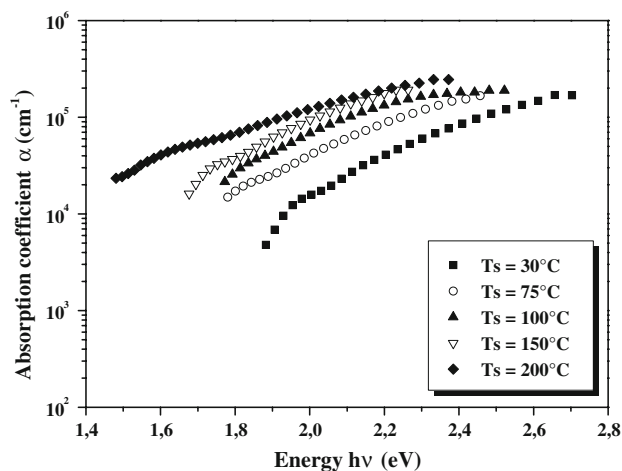


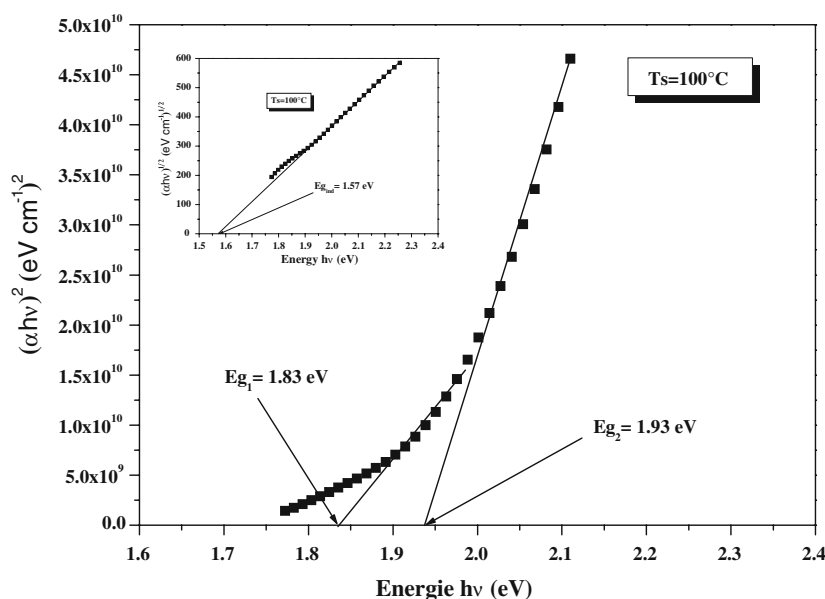
Fig. 8 Absorption coefficient spectra of CuIn_3S_5 films deposited at different substrate temperatures

The dependence of the absorption coefficient on photon energy is analysed in the high absorption regions to obtain detailed information about the energy band gaps. The absorption coefficient α and photon energy can be related by applying the model postulated by Davis and Mott [29]:

$$\alpha hv = A(hv - E_g)^n \quad (5)$$

where A is a constant that depends on the transition probability, h is the Planck constant and n is a number that characterizes the optical absorption process ($n = 1/2$ for a direct allowed transition and $n = 2$ for an indirect allowed transition). We plot $(\alpha hv)^2$ and $(\alpha hv)^{1/2}$ against hv (Fig. 9). Values of the direct and indirect optical energy gaps E_g^d and E_g^{ind} for films are obtained by extrapolating the linear regions of the $(\alpha hv)^2$ and $(\alpha hv)^{1/2}$ versus hv curve to the

Fig. 9 Plot of $(\alpha hv)^2$ versus hv for CuIn_3S_5 films deposited 100 °C. The inset shows the of $(\alpha hv)^{1/2}$ versus hv for CuIn_3S_5 films deposited at 100 °C



horizontal photon energy axis. Two direct allowed transitions for each sample: E_{g1} and E_{g2} , due to p - d hybridization of the valence band in chalcopyrite compound, were found. E_{g1} corresponds to the valence band–conduction band transition (the optical band gap), the transition with E_{g2} is associated with valence band splitting under the influence of the crystal field of lattice Δ_{CF} . This type of behaviour was also observed in other chalcopyrite compounds [30, 31]. All the values determined for the samples were summarized in Table 3. Figure 9 and Table 3 show a decrease in the values of the direct and indirect energy gaps of CuIn_3S_5 thin films by increasing the substrate temperature.

However, this decrease in these optical band gaps can be attributed to the improvement of crystallinity and the increase in particle size by increasing the substrate temperature. Lower band gap values are often related to higher optical absorption coefficient [32, 33]. On the other hand, the conductivity type is determinate by the hot probe method and all samples are N -type conductivity except that which was deposited at $T_s = 200$ °C. This sample is highly compensated. Figure 10 shows the variation of film

Table 3 The estimated values of optical parameters for CuIn_3S_5 thin film

T_s (°C)	Thickness (nm)	E_g^d		E_g^{ind}
		E_{g1}	E_{g2}	
30	520	2.04	2.17	1.81
75	515	1.88	1.99	1.63
100	410	1.83	1.93	1.57
150	450	1.78	1.86	1.54
200	350	1.52	1.77	1.35

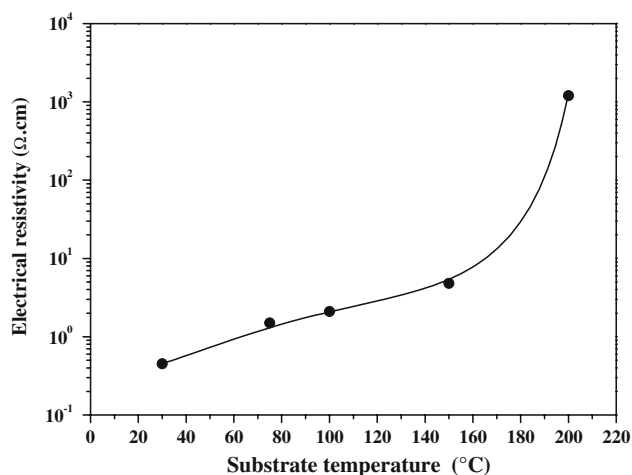


Fig. 10 Electrical resistivity of CuIn_3S_5 films deposited at different substrate temperatures

resistivity with deposition temperature. The resistivities drastically increase from 30 to 200 °C by increasing the substrate temperatures. One of the reasons may be that the increase in grain size by increasing the substrate temperature.

Conclusion

Ingots of CuIn_3S_5 material were obtained by the horizontal Bridgman method. Crushed powder of this ingot was used as raw material for the vacuum thermal evaporation. Therefore, CuIn_3S_5 thin films were deposited by vacuum thermal evaporation method on heated glass substrates. The as deposited CuIn_3S_5 thin films at substrate temperatures lower than 75 °C are amorphous, whereas those deposited on heated substrate higher than 75 °C show a polycrystalline structure with a preferred orientation along the (211) plane. In addition, improvement in the crystallinity was observed for the films deposited at high substrate temperatures. Surface topologies studied by AFM imaging show that grain size and surface RMS are affected by the substrate temperature. The analysis of the optical absorption spectra revealed two direct allowed transitions, which are attributed to the fundamental edge and band splitting by crystal field, respectively. All these properties confer to the material interest perspectives for its application in many physical domains such as optical, photovoltaic conversion and others.

References

- Krunks M, Bijakina O, Varema T, Mikli V, Mellikov E (1999) *Thin Solid Films* 338:125
- Djellal L, Bouguelia A, Trari M (2008) *J Semicond Sci Technol* 23:450
- Wasim SM, Rincon C, Marin G (2002) *Phys Status Solidi A* 194:244
- Ariswan, El Haj Moussa G, Abdelali M, Guastavino F, Llinares C (2002) *Solid State Commun* 124:391
- Zribi M, Kanzari M, Rezig B (2006) *Mater Lett* 60:98
- Guillen C (2006) *J Semicond Sci Technol* 21:709
- Malar P, Savitha Pillai S, Kasiviswanathan S (2007) *Mater Chem Phys* 101:118
- Zhang SB, Wei SH, Zunger A (1997) *Phys Rev Lett* 78:40
- Scheer R, Lewerenz HJ (1994) *J Vac Sci Technol A* 12:51
- Kato T, Omata T, Nakamura T, Anno D, Nabetani Y, Matsumoto T (2005) *J Cryst Growth* 275:531
- Cattarin S, Guerriero P, Dietz N, Lewerenz HJ (1994) *Electrochim Acta* 40:1041
- Berenguier B, Lewerenz HJ (2006) *Electrochem Commun* 8:165
- Scheer R, Lewerenz HJ (1995) *J Vac Sci Technol A* 13:1924
- Heavens OS (1950) *Optical properties of thin solid films*. Butterworths, London
- Mobaraka M, Shaban HT, Elhady AF (2008) *Mater Chem Phys* 109:287
- Korashy AE, Abdel-Rahim MA, El-Zahed H (1999) *Thin Solid Films* 338:207
- Diaz R, Bisson L, Agullo-Rueda F, Abd Lefdil M, Rueda F (2005) *Appl Phys A* 81:433
- Chang-Dae K, Moon-Seog J, Wha-Tek K (1998) *J Korean Phys Soc* 30:750
- Abernathy CR, Bates CW, Anani AA, Haba B, Smestad G (1984) *Appl Phys Lett* 45:890
- Bodnar IV, Victorov IA, Kushner TL, Rud VY, Rud YV (2005) *Thin Solid Films* 487:199
- Bodnar IV (2008) *Inorg Mater* 44:104
- Mamazza R Jr, Morel DL, Ferekides CS (2005) *Thin Solid Films* 484:26
- Warren BE (1990) *X-ray diffraction*. Dover, New York, p 253
- Revathi N, Prathap P, Ramakrishna Reddy KT (2008) *Appl Surf Sci* 254:5291
- Djessas K, Masse G, Ibannaim M (2000) *J Electrochem Soc* 147:1235
- Ye JD, Gu SL, Zhu SM, Qin F, Hu LQ, Ren L, Zhang R, Shi Y, Zheng YD (2004) *Appl Phys A* 78:761
- Milovzorov DE, Ali AM, Inokuma T, Kurata Y, Suzuki T, Hasegawa S (2001) *Thin Solid Films* 382:47
- Kononov I (2004) *Thin Solid Films* 451–452:413
- Davis EA, Mott NF (1970) *Philos Mag* 22:903
- Reena Philip R, Pradeep B (2005) *Thin Solid Films* 472:136
- Tembhurkar YD, Hirde JP (1992) *Thin Solid Films* 215:65
- Guillén C (2006) *Semicond Sci Technol* 21:709
- Kanzari M, Rezig B (2000) *Semicond Sci Technol* 15:335